Thin Solid Films 577 (2015) 103–108

Contents lists available at ScienceDirect

Thin Solid Films

journal homepage: www.elsevier.com/locate/tsf

Preparation and characterization of dye-sensitized TiO_2 nanorod solar cells

Lijian Meng [a,b,*], Hong Chen [c], Can Li [d], M.P. dos Santos [e,f]

[a] Departamento de Física, Instituto Superior de Engenharia do Porto, Instituto Politécnico do Porto, Rua Dr. António Bernardino de Almeida, 431, 4200-072 Porto, Portugal
[b] Centro de Física, Universidade do Minho, 4800-058 Guimarães, Portugal
[c] Key Laboratory of Optical System Advanced Manufacturing Technology, Changchun Institute of Optics, fine Mechanics and Physics of Chinese Academy of Science, Changchun 130033, China
[d] State Key Laboratory of Catalysis, Dalian Institute of Chemical Physics, Chinese Academy of Sciences, 457 Zhongshan Road, Dalian 116023,China
[e] CEFITEC, Faculdade de Ciências e Tecnologia da Universidade Nova de Lisboa, 2829-516 Caparica, Portugal
[f] Departamento de Física, Escola de Ciências e Tecnologia, Universidade de Évora, Portugal

ARTICLE INFO

Article history:
Received 14 June 2014
Received in revised form 19 January 2015
Accepted 28 January 2015
Available online 7 February 2015

Keywords:
Titanium dioxide
Nanorods
Sputtering
Dye sensitized solar cells

ABSTRACT

TiO_2 nanorods were prepared by DC reactive magnetron sputtering technique and applied to dye-sensitized solar cells (DSSCs). The length of the TiO_2 nanorods was varied from 1 μm to 6 μm. The scanning electron microscopy images show that the nanorods are perpendicular to the substrate. Both the X-ray diffraction patterns and Raman scattering results show that the nanorods have an anatase phase; no other phase has been observed. (101) and the (220) diffraction peaks have been observed for the TiO_2 nanorods. The (101) diffraction peak intensity remained constant despite the increase of nanorod length, while the intensity of the (220) diffraction peak increased almost linearly with the nanorod length. These nanorods were used as the working electrodes in DSSCs and the effect of the nanorod length on the conversion efficiency has been studied. An optimum photoelectric conversion efficiency of 4.8% has been achieved for 4 μm length nanorods.

1. Introduction

A dye-sensitized solar cell (DSSC) is a promising device for using solar energy because of its low production cost compared to those of conventional semiconductor solar cells, and also its high light to electricity conversion efficiency [1–3]. The conventional DSSC consists of a dye-sensitized nanoporous TiO_2 coating on the transparent conducting oxide substrate as an electrode, electrolytes containing I^-/I_3^- redox couple and filling the pores of the TiO_2 electrode, and a platinum counter electrode placed on the top of it. The nanoporous electrodes are generally prepared by TiO_2 nanoparticles (25 nm in diameter) by sol-gel process [4,5]. The main advantage of this nanoporous structure is its huge surface area (more than 1000 times compared to the conventional polycrystalline film), which can increase significantly the dye adsorption and improve the photoelectric conversion efficiency. However, despite its high surface area, the disordered nanoporous structure results in a short electron diffusion length because of the electron traps at the contacts between nanoparticles. The diffusion coefficient of an electron in the anatase TiO_2 nanoparticle film is several orders of magnitude lower than that in anatase TiO_2 single crystal, which limits the power conversion efficiency [6,7]. To increase the diffusion coefficient of the electrons and improve the charge transport, DSSCs using one-dimensional (1-D) structures of TiO_2 as electrodes, such as nanotubes, nanorods and nanowires, have been recently reported [8–21]. These 1-D structures will enhance the electron transport due to the features of highly decreased particle to particle contacts and elongated structure with the specified directionality [12]. Generally, these 1-D structures are made by chemical methods and a high temperature treatment is needed, which is not suitable for flexible DSSCs [13–15,17,18,20]. Magnetron sputtering technique has been considered as an adequate method for large area deposition with high uniformity at a relatively low deposition temperature. The sputtering process is easily controlled and reproduced. Generally, the TiO_2 film prepared by sputtering technique has a very compact structure, which is not suitable for DSSC applications. In our previous works, TiO_2 films with the nanorod structure have been prepared by dc reactive magnetron sputtering by adjusting the sputtering parameters and were applied as electrodes in DSSCs applications [22–26]. In this paper, the effect of the nanorod length on the structure properties of the TiO_2 films is reported. The DSSCs have been assembled using the TiO_2 films with different nanorod lengths and the effect of the nanorod length on the photoelectric properties has been studied.

2. Experimental details

The TiO_2 nanorod films were prepared on the commercial indium-tin oxide (ITO) substrates (sheet resistance of 20 Ω per square and thickness of 100 nm) by dc reactive magnetron sputtering technique using a commercial sputtering system equipped with a turbo molecular

* Corresponding author.
E-mail address: ljm@isep.ipp.pt (L. Meng).

http://dx.doi.org/10.1016/j.tsf.2015.01.064
0040-6090/

pumping system. A titanium metal disk (60 mm in diameter and 3 mm in thickness) with a purity of 99.99% was used as the target. After pumping down the system to 1×10^{-3} Pa, the oxygen and argon gases (99.99% purities) were introduced into the chamber through the mass flow controllers. The oxygen partial pressure and the total sputtering pressure were kept at 0.25 Pa and 2.00 Pa, respectively. The target-substrate distance was 45 mm. The deposition time was varied to obtain the film with different nanorod lengths. The sputtering was carried out using a constant current mode. The sputtering current was kept at 0.56 A and the cathode potential was about 420 V. In order to remove the surface contaminants of the target, pre-sputtering was done for 20 min with a shutter covering the substrate. The transmittance of the films was measured using a Jasco V-550 UV–Vis spectrophotometer. The X-ray diffraction (XRD) measurements have been done using Rigaku miniflex goniometer for the 2θ ranging from 20° to 75° with a step of 0.02° using Cu Ka radiation operated at 30 kV and 15 mA as the incident radiation. The morphologies of the nanorods were studied using field emission scanning electron microscope (FE-SEM) with an operating voltage of 20 kV. Raman scattering measurements have been done using a semiconductor laser and a 532 nm laser line was used as exciting light. The laser line was focused on the sample surface in a strict 180° backscattering geometry.

The TiO_2 films were sensitized with N719 (Ru(II)L2(NCS)2:2TBA, where L = 2,2′-bipyridyl-4,4′-dicarboxylic acid) dye by soaking the films in an ethanolic solution of N719 dye (0.5 mM) for 24 h at room temperature. The sputtered Pt film with 100 nm thickness and 0.3 nm/s deposition rate on an FTO glass substrate was used as the counter-electrode. The electrolyte was composed of 0.1 M I_2, 0.1 M LiI, 0.6 M 1-hexyl-3-methylimidazolium iodide, and 0.5 M 4-tert-butylpyridine in 3-methoxypropionitrile. The photocurrent-voltage measurements were carried out with a Princeton 2273 Applied Research electrochemical system, a 500 W Xenon lamp under AM 1.5G illumination with a water filter was used. The light intensity was adjusted to 100 mW/cm^2. Cells with an active area of 0.15 cm^2 were tested.

3. Results and discussion

Fig. 1 shows the FE-SEM images of TiO_2 films with different nanorod lengths. The SEM images show vertically well-aligned densely-packed TiO_2 nanorods grown on ITO substrate. No clear variations of the structure and the dimension of these nanorods can be observed from the images with the increase of the nanorod length. Thornton suggested the zone classification by considering the final working pressure, because this growth parameter can change both the kinetic energy of the ions that arrive at the substrate and the mean free path of the particles, which allows an increase or decrease in the bombardment of the surface of the substrate, that determines the mobility of the adatoms in that surface [27]. The microstructure of the films prepared by sputtering is determined by the adatom surface mobility during the growth. At high sputtering pressure, the kinetic energy of the argon ions will be reduced due to the decrease of the mean free path and results in a very low adatom mobility. Therefore, the structure is dominated by shadowing effects that overcome limited adatom surface diffusion. The most of the sputtered fluxes are deposited on high points on the film, with little material reaching the valleys and will result in the evolution of voids surrounding the rod-shaped columns structure – nanorod array.

Fig. 2a shows the XRD patterns of the TiO_2 films with different nanorod lengths. All the films show an anatase phase and a preferred

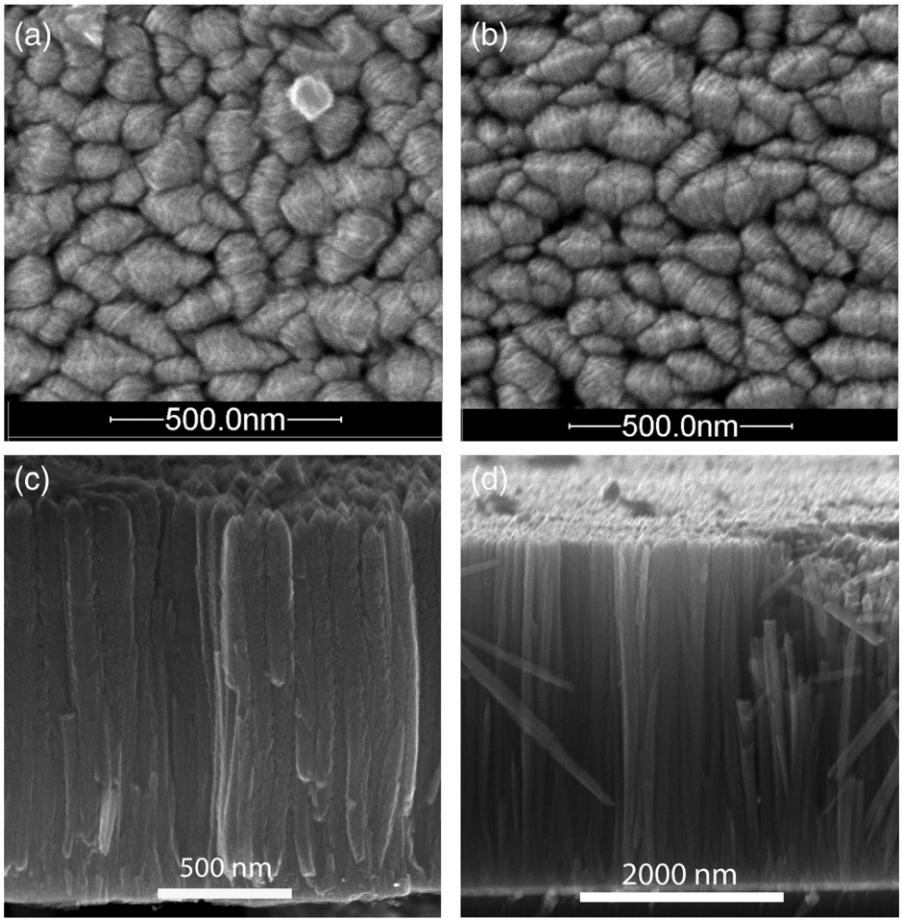

Fig. 1. FE-SEM images of two TiO_2 films with different nanorod lengths (1850 nm and 4770 nm). (a) and (b): surface views; (c) and (d): cross-section views.

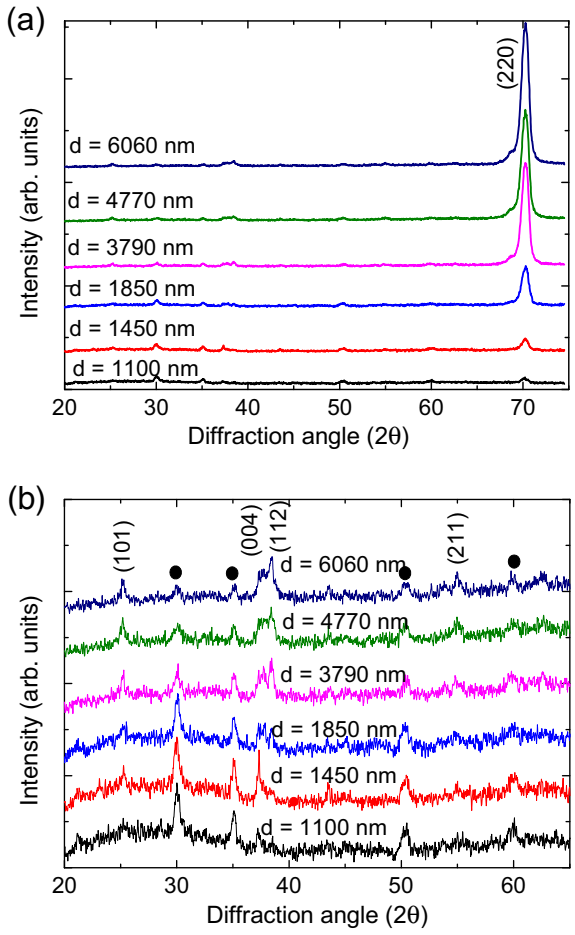

Fig. 2. X-ray diffraction patterns of the sputtered TiO_2 films with the different nanorod lengths. (a) The panorama patterns; (b) the patterns without the (220) diffraction peak. (The black solid circles represent the diffraction peaks from ITO).

orientation along the [110] direction. It can be seen that the (220) diffraction peak intensity increases with the nanorod length. The relative intensity of this diffraction peak is very strong which makes impossible to distinguish the diffraction peaks corresponding to other planes. In order to see the other diffraction peaks, the XRD patterns of the samples without (220) diffraction peak have been presented in Fig. 2b. The other diffraction peaks from the anatase TiO_2 can be observed in this figure. However, the intensities of these diffraction peaks do not show a very clear variation with the nanorod length. The intensity ratio of I(220)/I(101) has been calculated for TiO_2 films with different nanorod lengths and shown in Fig. 3. A linear increase of the ratio with the nanorod length can be observed. It means that the nanorod structure is favorable for the growth along the [110] direction. The thermodynamic model is generally used to explain the preferential growth direction of the films [28]. In the thermodynamic model, it has been established that the growth orientation in thin films is obtained at the thermodynamic equilibrium, which will be reached when the total energy - the sum of surface energy and deformation energy - of the system substrate-film has a minimum. The preferred orientation is determined by a configuration of minimum total energy, which results from competition between the planes with minimum deformation energy, and the planes with minimum surface energy. The average surface energies of the [110], [001], [100] and [101] crystal planes of anatase TiO_2 are 1.09 J/m^2, 0.90 J/m^2, 0.53 J/m^2 and 0.44 J/m^2, respectively [29]. In general, based on the Wulff construction, according to which surface energy minimization drives the optimal composition of the crystal surface, the (101) plane and the (001) plane were shown to be the most thermodynamically stable planes of anatase crystallites [30,31], which is also in agreement with the natural minerals. However, the diffraction intensity of the (101) plane is very small in all the samples. It suggests that the preferred orientation along the [110] direction is not dominated by the minimum surface energy but by the minimum deformation energy. It has be found that, in sufficiently thin films, the surface and interface energy minimizing textures are favored, regardless of their strain or thermal history, and in thick films the deformation energy minimizing textures are favored [32]. This implies that the preferred orientation along the [110] direction is dominated by the deformation energy minimizing as the peak intensity increases with the thickness. The grain sizes along the (110) direction have been estimated from Scherrer's formula based on the XRD data. All the TiO_2 films with different nanorod lengths present a similar grain size value of 24 nm. It means that the increase of the growing time does not increase the grain dimension, but increases the number of grains, and results in an increase of the nanorod length.

Fig. 4 presents the Raman spectra of TiO_2 films with different nanorod lengths. Five anatase TiO_2 Raman peaks can be observed clearly in the spectra which are in agreement with the results of XRD. The peaks at around 144, 195, and 637 cm^{-1} are attributed to E_g modes; the peak at 396 cm^{-1} is assigned to B_{1g} mode; and the peak at 513 cm^{-1} consists of two modes, $A_{1g} + B_{1g}$ [33]. The increase of the nanorod length does not bring any more effects on Raman spectra except for the peak intensity. The peak intensity increases gradually with the nanorod length.

The specular transmittance of the TiO_2 films with different nanorod lengths are presented in Fig. 5. It can be seen that the transmittance decreases with the increase of the nanorod length. The decrease of the

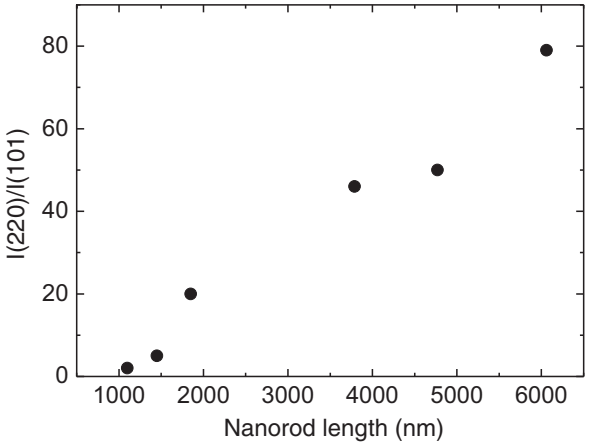

Fig. 3. Variation of I(220)/I(101) with the nanorod length.

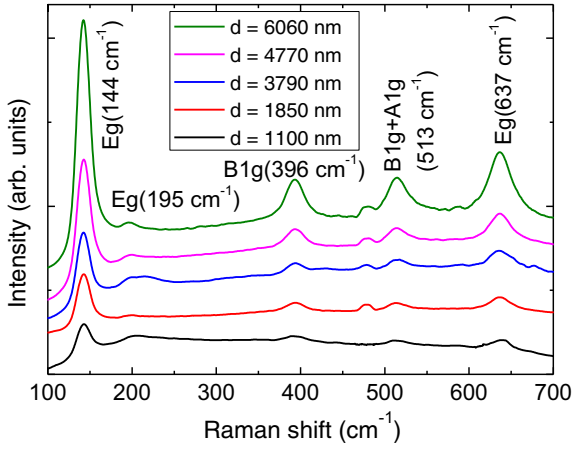

Fig. 4. Raman spectra of TiO_2 films with different nanorod lengths.

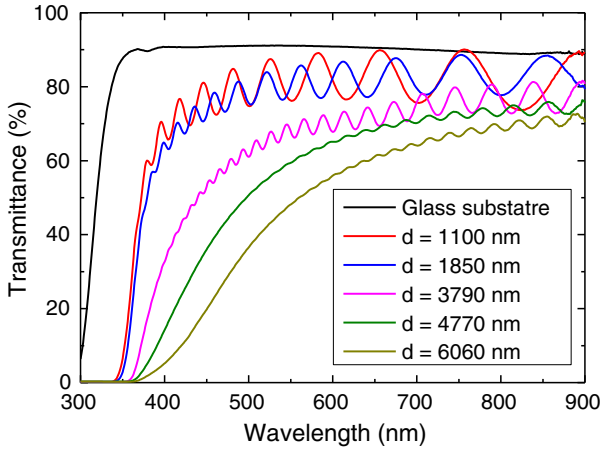

Fig. 5. The optical transmittance spectra of TiO_2 films with different nanorod lengths.

transmittance may result from the grain boundary scattering. As all the samples have a similar structure except for the nanorod length, the film with longer nanorod length has more grains along the [110] direction and this may result in an increase of the possibility of light scattering between the grain boundaries. Fig. 5 shows that the optical absorption edge of the TiO_2 films has a red shift as the nanorod length is increased, which indicates a decrease of the optical band gap. An indirect transition between the top of the valence band and the bottom of the conduction band is supposed for estimating the optical band gap E_g of the TiO_2 films with different nanorod lengths using the relation [34]

$$(\alpha h\nu)^{\frac{1}{2}} \propto \left(h\nu - E_g\right) \tag{1}$$

where $h\nu$ is the photon energy and α is the absorption coefficient. The α can be calculated using the relation

$$\alpha = -\frac{lnT}{d} \tag{2}$$

where T is the transmittance and d is the nanorod length. The optical band gap of the TiO_2 films was determined from the extrapolation of the linear plot of $(\alpha h\nu)^{\frac{1}{2}}$ versus $h\nu$ at $\alpha = 0$. The optical band gap of the TiO_2 films with different nanorod lengths is presented in Fig. 6. The optical band gap of the films decreases from 3.25 eV to 2.65 eV as the nanorod length is increased from 1100 nm to 6060 nm. The decrease of the optical band gap with the increase of the film thickness has been observed not only for TiO_2 films but also for other kind of films [35–38].

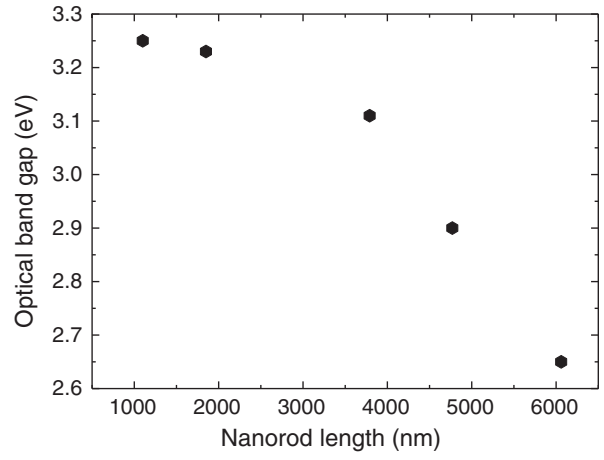

Fig. 6. Variation of optical band gap with the nanorod length.

The band gap is an optical property that is influenced by crystallographic parameters such as order and strain on the atomic level. The decrease of band gap with the increase of thickness is generally attributed to the increase of crystallite size and decrease in strain and dislocation density [39–41]. For our TiO_2 films with different nanorod lengths, the grain size along the [110] direction and the distance between the (220) planes have been calculated. The grain size is about 24 nm and the distance between the (220) planes is 0.1339 nm, which is quite similar to the standard value (0.1338 nm, PDF card 21-1272) for all the samples. It means that the modification of the optical band gap in our samples cannot be explained by strain and dislocation density. In general, the amorphous phase has a larger optical band gap than the polycrystalline phase for the same material [42,43]. It can be seen from the Fig. 2 that the films with short nanorod length show a relatively weak diffraction peak intensity. This suggests that an amorphous phase coexists in the films, and results in the larger optical band gap. The percentage of the amorphous phase decreases with the increase of the nanorod length and results in a decrease of the optical band gap as shown in Fig. 6.

The DSSCs have been assembled using these TiO_2 films with different nanorod lengths as the electrodes and the photocurrent density–photovoltaic performance of DSSCs is shown in Fig. 7. It can be seen that the photocurrent density increases as the nanorod length is increased from 1100 nm to 3790 nm and decreases as the nanorod length is increased further. The open-circuit voltage has a very small variation with the nanorod length. The DSSC with 6060 nm length of nanorod shows the worst fill factor. The variations of the short-circuit current density, J_{sc}; open-circuit voltage, V_{oc}; fill factor, FF; and conversion efficiency η with nanorod length are shown in Fig. 8. It can be seen that the photocurrent density governs the conversion efficiency of the DSSCs. The DSSC with a maximum photocurrent density has a maximum conversion efficiency (4.82%), which was achieved for DSSC assembled using a TiO_2 film with 3790 nm nanorod length. This efficiency is higher than the work reported by Liu et al. [14] who used single-crystalline rutile TiO_2 nanorods prepared by a hydrothermal method as the electrodes. The efficiency of 3% has been achieved by using 4 μm-long TiO_2 nanorod films. However, a conversation efficiency of 9.52% has been achieved by using 14 μm thickness TiO_2 nanorod film prepared by electrospinning as reported by Lee et al. [18]. Although the conversion efficiency of this work is still not so high as some reported results using TiO_2 nanorods as electrodes, it is the best one for DSSC using TiO_2 nanorod prepared by magnetron sputtering method until now. The photocurrent density will be generally decided by two factors: generation and transport of the photoelectrons. The generation of the photoelectrons is related to the amount of the dye adsorbed on the TiO_2 nanorods. In order to get a qualitative information on the dye adsorption, the transmittance of dye-sensitized TiO_2 films with different

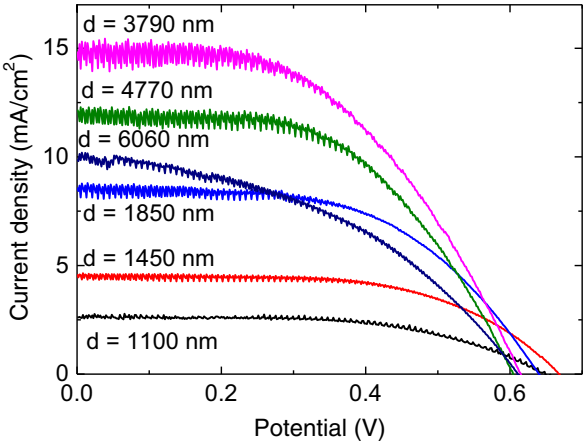

Fig. 7. Comparison of the J–V characteristics of DSSCs using TiO_2 films with different nanorod lengths as the electrodes.

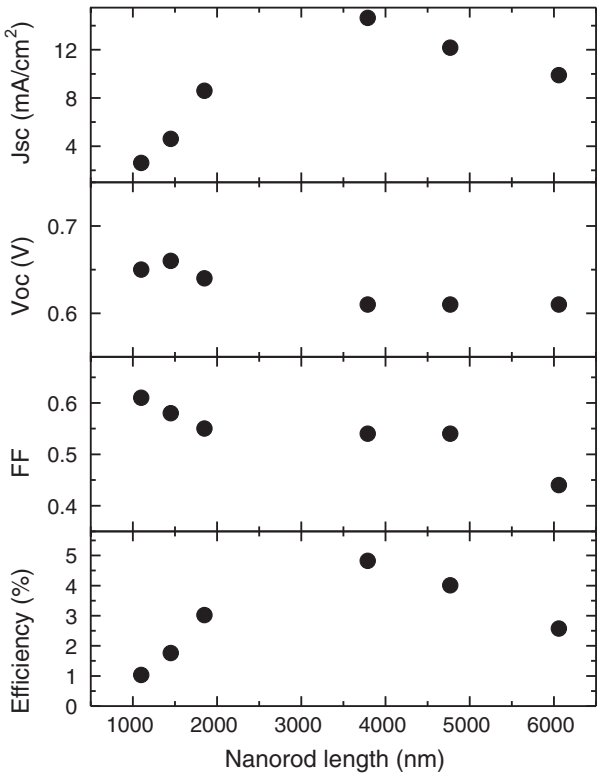

Fig. 8. Variation of solar cell parameters, short circuit current density Jsc, open circuit voltage Voc, fill factor and conversion efficiency with the nanorod length.

nanorod lengths have been measured as shown in Fig. 9. It can be seen that the dye adsorption shows a very clear increase as the nanorod length is increased from 1100 nm to 3790 nm. However, the dye adsorption does not increase obviously as the nanorod length is increased from 3790 nm to 6060 nm. It can be seen from the Fig. 1 that these TiO_2 nanorods are packed very closely, the voids among the nanorods are very small, and the dye molecules can only get into the voids by the phenomenon of capillary siphon. The maximum depth which the dye molecules can reach under these experimental conditions may be limited to the certain value and the further increase of the nanorod length may have no contribution on the dye adsorption. This results in a saturation of the dye adsorption at 3790 nm length. On the other hand, further increasing the nanorod length will also

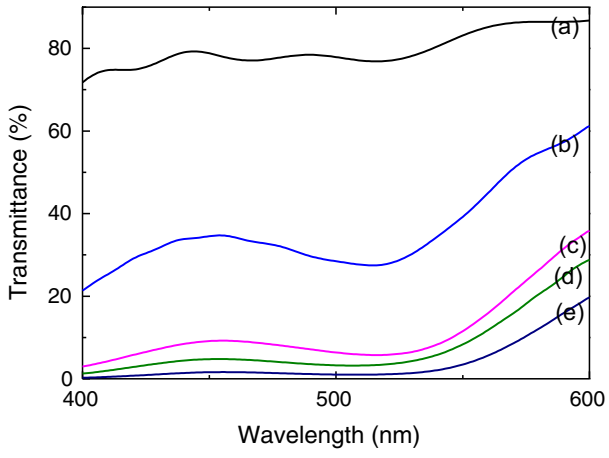

Fig. 9. The optical transmittance spectra of TiO_2 films with different nanorod lengths after dye-adsorption. The nanorod lengths are 1100 nm, 1850 nm, 3790 nm, 4770 nm and 6060 nm for (a), (b), (c), (d) and (e) respectively.

increase the electron diffusion path length and will result in the increase of the possibility of the recombination of the electrons. It will decrease the photocurrent density as shown in Fig. 8.

4. Conclusions

TiO_2 films with vertically well-aligned densely-packed nanorods structure have been prepared on the ITO substrates by dc reactive magnetron sputtering. TiO_2 films with different nanorod lengths have been prepared. The variation of the nanorod length does not affect the nanorod structure. The nanorods show a preferred orientation along the [110] direction. The increase of the nanorod length enhances this orientation. The thermodynamic model has been used to explain the preferred orientation. The optical band gap decreases as the nanorod length is increased. DSSCs have been assembled using the TiO_2 films with different nanorod lengths as electrodes and the maximum conversion efficiency of 4.82% has been achieved for DSSC using a TiO_2 film with 3790 nm nanorod length.

References

[1] B. Oregan, M. Gratzel, A low-cost, high-efficiency solar-cell based on dye-sensitized colloidal TiO_2 films, Nature 353 (1991) 737.
[2] M. Gratzel, Solar energy conversion by dye-sensitized photovoltaic cells, Inorg. Chem. 44 (2005) 6841.
[3] M. Gratzel, Future development of technology in dye-sensitized solar cells, Electrochemistry 79 (2011) 760.
[4] M.D. Wei, Y. Konishi, H.S. Zhou, M. Yanagida, H. Sugihara, H. Arakawa, Highly efficient dye-sensitized solar cells composed of mesoporous titanium dioxide, J. Mater. Chem. 16 (2006) 1287.
[5] D.H. Chen, F.Z. Huang, Y.B. Cheng, R.A. Caruso, Mesoporous anatase TiO_2 beads with high surface areas and controllable pore sizes: a superior candidate for high-performance dye-sensitized solar cells, Adv. Mater. 21 (2009) 2206.
[6] L. Forro, O. Chauvet, D. Emin, L. Zuppiroli, H. Berger, F. Levy, High-mobility N-type charge-carriers in large single-crystals of anatase (TiO_2), J. Appl. Phys. 75 (1994) 633.
[7] B. Enright, D. Fitzmaurice, Spectroscopic determination of electron and mole effective masses in a nanocrystalline semiconductor film, J. Phys. Chem. U. S. 100 (1996) 1027.
[8] M. Zukalova, L. Kavan, J. Prochazka, A. Zukal, J.H. Yum, M. Graetzel, Nanofibrous TiO_2 improving performance of mesoporous TiO_2 electrode in dye-sensitized solar cell, J. Nanoparticle Res. 15 (2013) (Article:1640).
[9] B.E. Ahn, H.S. Kim, S.K. Yang, K.S. Ahn, S.H. Kang, Double layered nanoarchitecture based on anodic TiO_2 nanotubes for dye-sensitized solar cells, J. Photochem. Photobiol. A 274 (2014) 20.
[10] C. Zha, L. Shen, X. Zhang, Y. Wang, B.A. Korgel, A. Gupta, N. Bao, Double-sided brush-shaped TiO_2 nanostructure assemblies with highly ordered nanowires for dye-sensitized solar cells, ACS Appl. Mater. Interfaces 6 (2014) 122.
[11] J. Zhang, S.Q. Li, H. Ding, Q.T. Li, B.Y. Wang, X.N. Wang, H. Wang, Transfer and assembly of large area TiO_2 nanotube arrays onto conductive glass for dye sensitized solar cells, J. Power Sources 247 (2014) 807.
[12] M. Adachi, Y. Murata, J. Takao, J. Jiu, M. Sakamoto, F. Wang, Highly efficient dye-sensitized solar cells with a titania thin-film electrode composed of a network structure of single-crystal-like TiO_2 nanowires made by the "oriented attachment" mechanism, J. Am. Chem. Soc. 126 (2004) 14943.
[13] J.T. Jiu, S. Isoda, F.M. Wang, M. Adachi, Dye-sensitized solar cells based on a single-crystalline TiO_2 nanorod film, J. Phys. Chem. B 110 (2006) 2087.
[14] B. Liu, E.S. Aydil, Growth of oriented single-crystalline rutile TiO_2 nanorods on transparent conducting substrates for dye-sensitized solar cells, J. Am. Chem. Soc. 131 (2009) 3985.
[15] Y. Suzuki, S. Ngamsinlapasathian, R. Yoshida, S. Yoshikawa, Partially nanowire-structured TiO_2 electrode for dye-sensitized solar cells, Cent. Eur. J. Chem. 4 (2006) 476.
[16] L. Sun, S. Zhang, X. Sun, X. He, Effect of the geometry of the anodized titania nanotube array on the performance of dye-sensitized solar cells, J. Nanosci. Nanotechnol. 10 (2010) 4551.
[17] S. Ngamsinlapasathian, S. Sakulkhaemaruethai, S. Pavasupree, A. Kitiyanan, T. Sreethawong, Y. Suzuki, S. Yoshikawa, Highly efficient dye-sensitized solar cell using nanocrystalline titania containing nanotube structure, J. Photochem. Photobiol. A 164 (2004) 145.
[18] B.H. Lee, M.Y. Song, S.Y. Jang, S.M. Jo, S.Y. Kwak, D.Y. Kim, Charge transport characteristics of high efficiency dye-sensitized solar cells based on electrospun TiO_2 nanorod photoelectrodes, J. Phys. Chem. C 113 (2009) 21453.
[19] M. Law, L.E. Greene, J.C. Johnson, R. Saykally, P. Yang, Nanowire dye-sensitized solar cells, Nat. Mater. 4 (2005) 455.
[20] Y. Ohsaki, N. Masaki, T. Kitamura, Y. Wada, T. Okamoto, T. Sekino, K. Niihara, S. Yanagida, Dye-sensitized TiO_2 nanotube solar cells: fabrication and electronic characterization, Phys. Chem. Chem. Phys. 7 (2005) 4157.

[21] V. Thavasi, V. Renugopalakrishnan, R. Jose, S. Ramakrishna, Controlled electron injection and transport at materials interfaces in dye sensitized solar cells, Mater. Sci. Eng. R 63 (2009) 81.
[22] L. Meng, A. Ma, P. Ying, Z. Feng, C. Li, Sputtered highly ordered TiO_2 nanorod arrays and their applications as the electrode in dye-sensitized solar cells, J. Nanosci. Nanotechnol. 11 (2011) 929.
[23] L.J. Meng, C. Li, Blocking layer effect on dye-sensitized solar cells assembled with TiO_2 nanorods prepared by dc reactive magnetron sputtering, Nanosci. Nanotechnol. Lett. 3 (2011) 181.
[24] L.J. Meng, C. Li, M.P. dos Santos, Effect of annealing temperature on TiO_2 nanorod films prepared by dc reactive magnetron sputtering for dye-sensitized solar cells, J. Inorg. Organomet. Polym. Mater. 21 (2011) 770.
[25] L.J. Meng, C. Li, M.P. dos Santos, Structural modification of TiO_2 nanorod films with an influence on the photovoltaic efficiency of a dye-sensitized solar cell (DSSC), J. Inorg. Organomet. Polym. Mater. 23 (2013) 787.
[26] L.J. Meng, T. Ren, C. Li, The control of the diameter of the nanorods prepared by dc reactive magnetron sputtering and the applications for DSSC, Appl. Surf. Sci. 256 (2010) 3676.
[27] J.A. Thornton, Influence of apparatus geometry and deposition conditions on structure and topography of thick sputtered coatings, J. Vac. Sci. Technol. 11 (1974) 666.
[28] I. Goldfarb, J. Pelleg, L. Zevin, N. Croitoru, Lattice distortion in thin-films of Ivb metal (Ti, Zr, Hf) nitrides, Thin Solid Films 200 (1991) 117.
[29] M. Lazzeri, A. Vittadini, A. Selloni, Structure and energetics of stoichiometric TiO_2 anatase surfaces (vol 63, art no 155409, 2001), Phys. Rev. B 65 (2002) (Article: 119901).
[30] U. Diebold, N. Ruzycki, G.S. Herman, A. Selloni, One step towards bridging the materials gap: surface studies of TiO_2 anatase, Catal. Today 85 (2003) 93.
[31] R.L. Penn, J.F. Banfield, Morphology development and crystal growth in nanocrystalline aggregates under hydrothermal conditions: insights from titania, Geochim. Cosmochim. Acta 63 (1999) 1549.
[32] C.V. Thompson, Structure evolution during processing of polycrystalline films, Annu. Rev. Mater. Sci. 30 (2000) 159.
[33] M. Giarola, A. Sanson, F. Monti, G. Mariotto, M. Bettinelli, A. Speghini, G. Salviulo, Vibrational dynamics of anatase TiO_2: polarized Raman spectroscopy and ab initio calculations, Phys. Rev. B 81 (2010) (Article: 174305).
[34] J.I. Pankove, Optical Processes In Semiconductor, Dover Publication Inc., New York, 1970.
[35] S. Velumani, X. Mathew, P.J. Sebastian, Structural and optical characterization of hot wall deposited $CdSe_xTe_{1-x}$ films, Sol. Energy Mater. Sol. Cells 76 (2003) 359.
[36] N. Nithya, S. Rugmini Radhakrishnan, Effect of thickness on the properties ZnO thin films, Adv. Appl. Sci. Res. 3 (2012) 4041.
[37] M.A. Mohammed, Correlation between thickness, grain size and optical band gap of CdI2 film, Eng. Technol. J. 27 (2009) 1174.
[38] C. Guillen, J. Herrero, Optical, electrical and structural characteristics of Al:ZnO thin films with various thicknesses deposited by DC sputtering at room temperature and annealed in air or vacuum, Vacuum 84 (2010) 924.
[39] C.B. Murray, D.J. Norris, M.G. Bawendi, Synthesis and characterization of nearly monodisperse Cde (E = S, Se, Te) semiconductor nanocrystallites, J. Am. Chem. Soc. 115 (1993) 8706.
[40] H.C. Ong, A.X.E. Zhu, G.T. Du, Dependence of the excitonic transition energies and mosaicity on residual strain in ZnO thin films, Appl. Phys. Lett. 80 (2002) 941.
[41] Y. Zhao, M.T. Zhou, Z.O. Li, Z.Y. Lv, X.Y. Liang, J.H. Min, L.J. Wang, W.M. Shi, Effect of strain on the structural and optical properties of Cu–N co-doped ZnO thin films, J. Lumin. 131 (2011) 1900.
[42] S.T. Tan, B.J. Chen, X.W. Sun, W.J. Fan, H.S. Kwok, X.H. Zhang, S.J. Chua, Blueshift of optical band gap in ZnO thin films grown by metal-organic chemical-vapor deposition, J. Appl. Phys. 98 (2005) (Article: 013505).
[43] D.K. Dwivedi, H.P. Pathak, N. Shukla, A. Kumar, Effect of thermal annealing on structure and optical band gap of amorphous $Se_{75-x}Te_{25}Sb_x$ thin films by vacuuam evaporation technique, J. Ovonic. Res. 10 (2014) 15.